## Appendix 1 Preoperative dual-energy computed tomography (DECT) did not delay radioiodine ablation in patients with papillary thyroid carcinoma (PTC)

Neck enhanced CT scans routinely require the use of iodine contrast agents to ensure optimal imaging, and potential delay in radioactive iodine (RAI) treatment will not cause adverse effect according to National Comprehensive Cancer Network guidelines (version 2018 and version 2020 V1) (47,48).

Yeh's study (7) showed that iodized contrast agents could optimize the neck enhanced CT images, and that iodine load usually leaded to only a slight delay in postoperative RAI ablation, which was negligible. RAI ablation was recommended for at least one month after an enhanced iodized contrast scan to ensure urinary iodine levels return to baseline (49). Chinese Society of Clinical Oncology expert consensus provided a similar guidance for the evaluation of 131I before the treatment for differentiated thyroid cancer (DTC). At present, there was no clear evidence that this delay adversely affected the prognosis of thyroid cancer.

It is well known that the thyroid gland is the main reservoir of iodine in the body, and even in patients undergoing enhanced CT before surgery, iodine level drops rapidly after total thyroidectomy (50). In addition, much of the recommendations against performing contrast-enhanced CT in thyroid cancer patients was based on studies using lipophilic contrast agents, which tended to be stored in adipose tissues for a long time. However, most centers used water-soluble ionic contrast agents currently (such as iohexol used in the current study), which were unlikely to be retained in extracellular fluids (50). Therefore, unless there was further iodine intake, the urinary iodine concentration (UIC) could quickly return to its previous equilibrium after DECT. Several studies (49-54) showed that the normalization time of UIC was 30 to 43 days. Besides, in routine practice, if the patients with PTC who came to our hospital for the surgery needed postoperative RAI therapy, the whole process "preoperative examination → thyroidectomy → postoperative rehabilitation and discharge → appointment and preparation before RAI therapy → admission for RAI therapy" required to be completed. The entire process took at least 6 weeks without any delay or interference call for, which was longer than the American Thyroid Association (ATA) guidelines. On the other hand, the 2015 ATA guidelines stated that postoperative RAI therapy should only be routinely administered in high-risk DTC; it was not recommended in low-risk DTC and was considered in intermediate-risk group (27). Moreover, a large number of studies (53-57) have shown that the timing of RAI therapy after thyroidectomy did not affect the overall survival or long-term prognosis.

In the current study, all patients who received DECT before surgery were assured of at least one month before undergoing 131I treatment after surgery, and according to the follow-up results, the delay had no significant adverse impact on the prognosis of patients.

## Appendix 2 The specific principles of operation for PTC patients

The general principles for the treatment of the solitary were as follows: (I) unilateral lobectomy was performed for primary lesion <1 cm; (II) for primary lesion with a diameter of 1–4 cm, total thyroidectomy was considered if preoperative imaging suggested extrathyroid invasion or unilateral lobectomy was considered if the thyroid capsule was intact; (III) for primary lesions >4 cm, total thyroidectomy should be considered; (IV) regardless of the diameter of the primary lesion, total thyroidectomy should be considered if preoperative imaging suggested the presence of lateral cervical lymph node metastasis.

The principles of central cervical lymph node (level VI) dissection were as follows: When the primary lesion was located in the left or right lobe of the thyroid gland, lymph nodes in the ipsilateral central cervical region were dissected. For these patients, we performed ultrasound follow-up for at least one year to confirm that there was no lymph node metastasis in the contralateral central region. When the primary lesion was located in the isthmus or proximal isthmus, bilateral central lymph node dissection was performed.

## Appendix 3 The detailed ultrasound and DECT protocols

In Hospital A, the ultrasound images were re-evaluated by two radiologists with 11 and 13 years of thyroid cancer ultrasound diagnosis experience, and the DECT images were re-reviewed by another two radiologists with 10 and 14 years of experience in thyroid cancer CT diagnosis. They were all blinded to pathological diagnosis.

Philips iU22, LOGIQ E9, SuperSonic Images AxiPlorer, Mylab Tweice, and RS80A color Doppler ultrasonic


https://dx.doi.org/10.21037/qims-24-284

diagnostic apparatus were used to perform the examination, equipping with L4–15 linear array probe, and the frequency was 4–15 Hz. All patients were scanned in a supine position with shoulders naturally drooped and hands placed on either side of the chest, leaving the neck fully exposed. Routine examination of thyroid gland and cervical lymph nodes was performed in combination with longitudinal and transverse scans. In Hospital B, LOGIC 7, logic 9, Prerius C, and UGEOWS80A color Doppler ultrasonic diagnostic apparatus were used to perform the examination.

After ultrasound examination, the included patients underwent DECT examination. It is worth mentioning that the CT equipments of the two hospitals were the same. The DECT parameters were basically the same.

The scan was performed in a supine position with the patient's upper limbs at each side of the body and the shoulders naturally hanging down. Position the cursor longitudinally on the central sagittal plane of the cervicothoracic region. Ask the patient to hold their breath during apnea. The positioning image was scanned firstly, and then the scanning baseline was determined. The scan covered the entire neck, including the thyroid gland and lymph node area of the neck, from the upper edge of the aortic arch to the lower edge of the mandible.

The patient's heart rate was closely monitored to ensure that it remained at an average level throughout the scan. DECT scan was performed by arterial-phase and venophase dual-energy mode ratio enhanced scanning. The scanning parameters were set according to the lowest possible concept to achieve reasonable radiation protection as much as possible. The specific parameters were as follows: tube current, 600 mA; helical thickness, 6 mm; helical pitch, 0.9; rotation speed, 0.28 s; detector width, 40 mm; collimation, 64 × 0.6 mm. To obtain a faster scanning speed and reduce the motion artifacts of neck and radiation dose, a faster rotation speed and a moderate pitch were selected in this study. The iodinated nonionic contrast agent (iohexol; 350 mg/mL iodine, SOMATOM Definition Flash, Siemens Healthcare, Forchheim, Germany) was administered through the right elbow median vein by a dual-head injector at a dose of 1 mL/kg with a flow rate of 3 mL/s. The total injection dose was 60–70 mL, followed by 40 mL saline at the same flow rate. When the venous condition was not good, the left median cubital vein was chosen for administration. Automatic trigger technique was used to determine the time of the arteerial phase scan. The start time of arterial phase scan was 25 s after scanning delay. The delay time of the venous scan was 20 s after the end of the arterial scan.

All the original images were reconstructed into contiguous axial images with a slice thickness of 1 mm, a field of view (FOV) of 200 mm, and a matrix of 512×512. The arterial and venous phases DECT data of were transferred to the Siemens Syngovia workstation (Syngo DE, Siemens Healthcare, Forchheim, Germany) and processed using the Liver VNC function keys to obtain the iodine maps.

## Appendix 4 Specific ultrasound images analysis method

The ultrasound parameters were re-evaluated by two thyroid radiologists with 11 and 13 years of clinical experience independently, who were blinded to the clinical information and pathological results.

We measured diameter, shape (wider-than-tall or taller-than-wide), and the ratio of capsular abutment over the lesion perimeter (A/P) using Image Pro Plus software (Media Cybernetics, Silver Spring, USA). Manually sketch the diameter of each PTC lesion on three adjacent layers showing the maximum diameter of the target lesion (*Figure S1A*). The average value from three measurements was taken for the final evaluation. The measurement of A/P in a thyroid lesion was calculated by the average ratio (1/2) on the transversal + longitudinal section of a nodule (*Figure S1B*) (58). The capsular abutment was defined as a lack of intervening tissue between PTC lesions and normal thyroid capsules, which was outlined with blue line. The capsular protrusion was defined as the disruption of the perithyroidal echogenic line between the primary site of PTC and the normal thyroid capsule on sonography, which was outlined with red line (58). A/P was measured three times by the two radiologists and averaged, respectively. A week later, the diameter and A/P of PTC lesions were re-test. Intra- and inter-observer consistency analyses were performed to ensure the data accuracy.

Except for diameter and A/P, other parameters were all categorical variables. Taller-than-wide was defined as the anteroposterior diameter of the nodule that was larger than its transverse diameter on a transverse plane (*Figure S1C*) (59). Calcification in the PTC lesion was divided into the following four forms: none and large comet-tail calcification, macrocalcification, rim calcification, and microcalcification. According to American College of Radiology (ACR) Thyroid Imaging, Reporting and Data System (TI-RADS) (60), microcalcification appears was very


https://dx.doi.org/10.21037/qims-24-284

small (≤1 mm) hyperechoic regions (13), macrocalcification appears was more extensive (>1 mm) hyperechoic regions and rim calcification was annular calcification in the tumor margin that looked like an eggshell (*Figure S1D-S1F*) (61). The two radiologists evaluated them respectively. When there was a disagreement, they reported to the superior doctor, chief physician with more than 20 years of work experience, and reached an agreement after discussion.

## Appendix 5 The region of interest (ROI) selection methods on DECT images

On DECT images, we measured four quantitative parameters, including iodine concentration (IC) of the thyroid primary lesion in the arterial and venous phases and IC of the common carotid artery (CCA) in the arterial and venous phases. Normalized IC (NIC) of the primary lesion was obtained through the formulation of IC in the primary lesion divided by IC in the CCA at the same level.

Firstly, in order to make accurate measurement, the image was enlarged under the premise of ensuring the clarity of the image. Secondly, in conjunction with enhanced images and iodine maps in the arterial and venous phases, layers that clearly and completely showed the maximum cross-sectional area of the primary lesion were selected. Combining the three-dimensional images, the primary lesion with the largest cross-sectional area was selected to measure. ROI was placed on the substantial part as large as possible, pay attention to avoid cystic degeneration, necrosis, calcification, or adjacent blood vessels (*Figure S1G-S1I*).

## Appendix 6 Specific category description of the variables used to construct the nomogram

To minimize the burden imposed on clinicians by additional measurements, the predictors were dichotomized. Before the nomogram was performed, we ensured that the six variables used to construct the nomogram were categorical variables.

Diameter was graded by values of ≤1 cm, 1–2 cm, 2–4 cm, >4 cm, according to the 8th American Joint Committee on Cancer tumor-node-metastasis staging systems (62). The shape was graded by wider-than-tall and taller-than-wide. A shape "taller-than-wide" was one of the main features predictive of malignancy (27). The presence of microcalcification was another main feature predictive of malignancy (27); therefore, calcification was graded by four different categories according to ACR TI-RADS as following, none or large comet-tail, macrocalcification, rim calcification, and microcalcification (60). It's worth noting that, since no calcification and large comet-tail calcification were both zero point according to ACR TI-RADS, we classified them into one category. A/P was graded by values of <25%, 25–50%, or >50%, proven by a previous study (58).

We calculated the cutoff values of IC in the arterial and the venous phases by the Medcalc software, which were 2.4 and 3.2 mg/mL (*Table S5*), respectively, and classified them into two categories accordingly.

## References


47. NCCN guidelines for thyroid cancinoma 2018. V1 (download from the official website).
48. NCCN Clinical Practice Guidelines in Oncology for thyroid carcinoma version 1.2020.
49. Padovani RP, Kasamatsu TS, Nakabashi CC, Camacho CP, Andreoni DM, Malouf EZ, Marone MM, Maciel RM, Biscolla RP. One month is sufficient for urinary iodine to return to its baseline value after the use of water-soluble iodinated contrast agents in post-thyroidectomy patients requiring radioiodine therapy. Thyroid 2012;22:926-30.
50. Mishra A, Pradhan PK, Gambhir S, Sabaretnam M, Gupta A, Babu S. Preoperative contrast-enhanced computerized tomography should not delay radioiodine ablation in differentiated thyroid carcinoma patients. J Surg Res 2015;193:731-7.
51. Nimmons GL, Funk GF, Graham MM, Pagedar NA. Urinary iodine excretion after contrast computed tomography scan: implications for radioactive iodine use. JAMA Otolaryngol Head Neck Surg 2013;139:479-82.
52. Sohn SY, Choi JH, Kim NK, Joung JY, Cho YY, Park SM, Kim TH, Jin SM, Bae JC, Lee SY, Chung JH, Kim SW. The impact of iodinated contrast agent administered during preoperative computed tomography scan on body iodine pool in patients with differentiated thyroid cancer preparing for radioactive iodine treatment. Thyroid 2014;24:872-7.
53. Scheffel RS, Zanella AB, Dora JM, Maia AL. Timing of Radioactive Iodine Administration Does Not Influence Outcomes in Patients with Differentiated Thyroid Carcinoma. Thyroid 2016;26:1623-9.
54. Tsirona S, Vlassopoulou V, Tzanela M, Rondogianni P, Ioannidis G, Vassilopoulos C, Botoula E, Trivizas P, Datseris I, Tsagarakis S. Impact of early vs late postoperative radioiodine remnant ablation on final outcome in patients with low-risk well-differentiated thyroid cancer. Clin



https://dx.doi.org/10.21037/qims-24-284

Endocrinol (Oxf) 2014;80:459-63.
55. Krajewska J, Jarzab M, Kukulska A, Czarniecka A, Roskosz J, Puch Z, Wygoda Z, Paliczka-Cieslik E, Kropinska A, Krol A, Handkiewicz-Junak D, Jarzab B. Postoperative Radioiodine Treatment within 9 Months from Diagnosis Significantly Reduces the Risk of Relapse in Low-Risk Differentiated Thyroid Carcinoma. Nucl Med Mol Imaging 2019;53:320-7.
56. Kim M, Han M, Jeon MJ, Kim WG, Kim IJ, Ryu JS, Kim WB, Shong YK, Kim TY, Kim BH. Impact of delayed radioiodine therapy in intermediate-/high-risk papillary thyroid carcinoma. Clin Endocrinol (Oxf) 2019;91:449-55.
57. Suman P, Wang CH, Abadin SS, Block R, Raghavan V, Moo-Young TA, Prinz RA, Winchester DJ. Timing of radioactive iodine therapy does not impact overall survival in high-risk papillary thyroid carcinoma. Endocr Pract 2016;22:822-31.
58. Wei X, Wang M, Wang X, Zheng X, Li Y, Pan Y, Li Y, Mu J, Yu Y, Li D, Gao M, Zhang S. Prediction of cervical lymph node metastases in papillary thyroid microcarcinoma by sonographic features of the primary site. Cancer Biol Med 2019;16:587-94.
59. Moon WJ, Jung SL, Lee JH, Na DG, Baek JH, Lee YH, Kim J, Kim HS, Byun JS, Lee DH; Thyroid Study Group, Korean Society of Neuro- and Head and Neck Radiology. Benign and malignant thyroid nodules: US differentiation--multicenter retrospective study. Radiology 2008;247:762-70.
60. Tessler FN, Middleton WD, Grant EG, Hoang JK, Berland LL, Teefey SA, Cronan JJ, Beland MD, Desser TS, Frates MC, Hammers LW, Hamper UM, Langer JE, Reading CC, Scoutt LM, Stavros AT. ACR Thyroid Imaging, Reporting and Data System (TI-RADS): White Paper of the ACR TI-RADS Committee. J Am Coll Radiol 2017;14:587-95.
61. Gharib H, Papini E, Garber JR, Duick DS, Harrell RM, Hegedüs L, Paschke R, Valcavi R, Vitti P; AACE/ACE/AME Task Force on Thyroid Nodules. American Association of Clinical Endocrinologists, American College Of Endocrinology, and Associazione Medici Endocrinologi Medical guidelines for clinical practice for the diagnosis and management of thyroid nodules--2016 update. Endocr Pract 2016;22:622-39.
62. Verburg FA, Mäder U, Luster M, Reiners C. The effects of the Union for International Cancer Control/American Joint Committee on Cancer Tumour, Node, Metastasis system version 8 on staging of differentiated thyroid cancer: a comparison to version 7. Clin Endocrinol (Oxf) 2018;88:950-6.


https://dx.doi.org/10.21037/qims-24-284

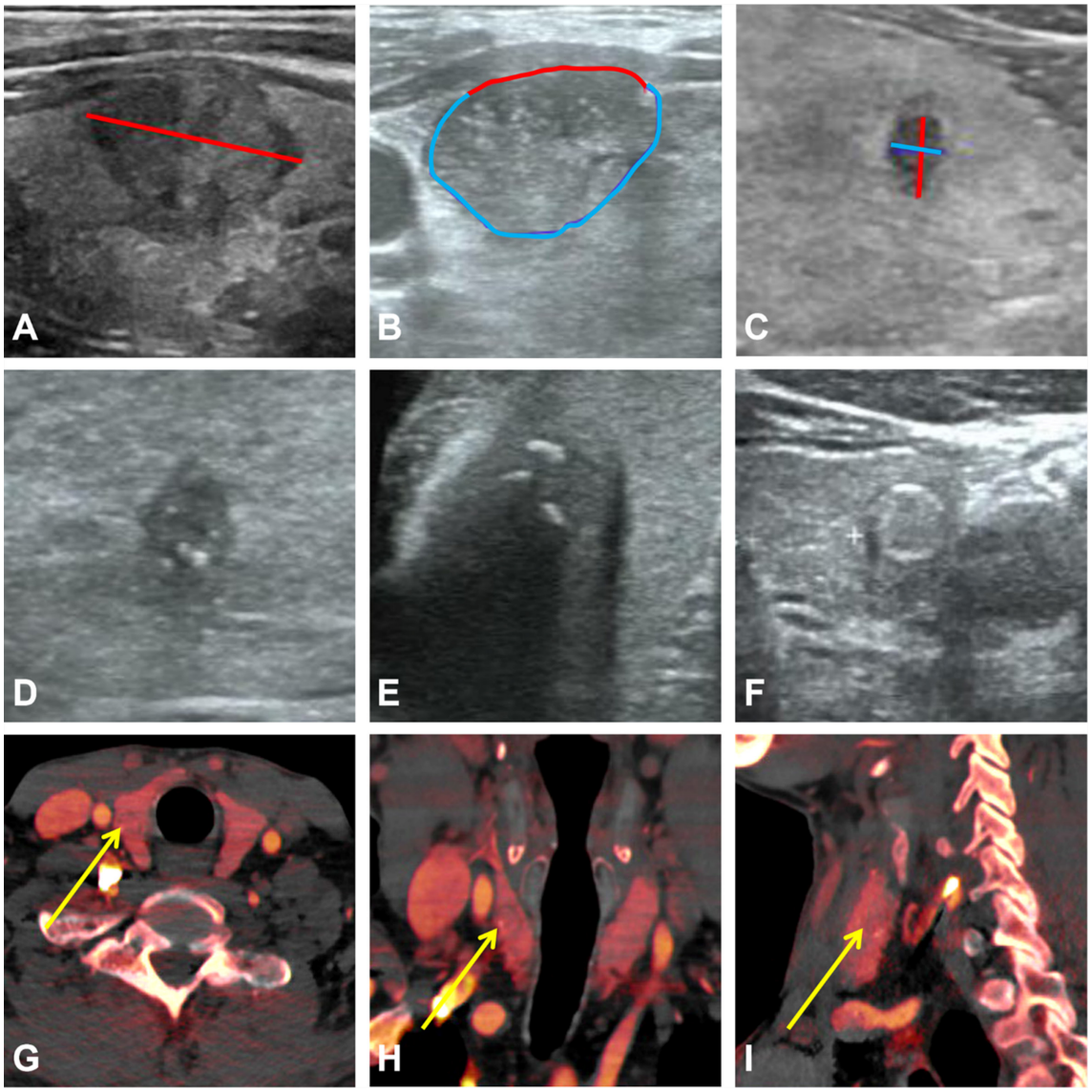


**Figure S1** Ultrasound and DECT images analysis method. (A) Diameter of the primary lesion. (B) Schematic diagram of the measurement of A/P of the primary lesion. The measurement of A/P in a thyroid lesion was calculated by the average ratio (1/2) on the transversal + longitudinal section of a nodule. The capsular abutment was defined as a lack of intervening tissue between PTC lesions and normal thyroid capsules, which was outlined with blue line. The capsular protrusion was defined as the disruption of the perithyroidal echogenic line between the primary site of PTC and the normal thyroid capsule on sonography, which was outlined with red line. (C) Taller-than-wide in the primary lesion, which was defined as the anteroposterior diameter of the nodule (blue line) that was larger than its transverse diameter (red line) on a transverse plane. (D) Microcalcification. (E) Macrocalcification. (F) Rim calcification. (G-I) Iodine maps of the primary focus on DECT in the axial, coronal, and sagittal positions, respectively. A/P, the ratio of capsular abutment over the lesion perimeter; DECT, dual-energy computed tomography; PTC, papillary thyroid carcinoma; ROI, region of interest.


https://dx.doi.org/10.21037/qims-24-284

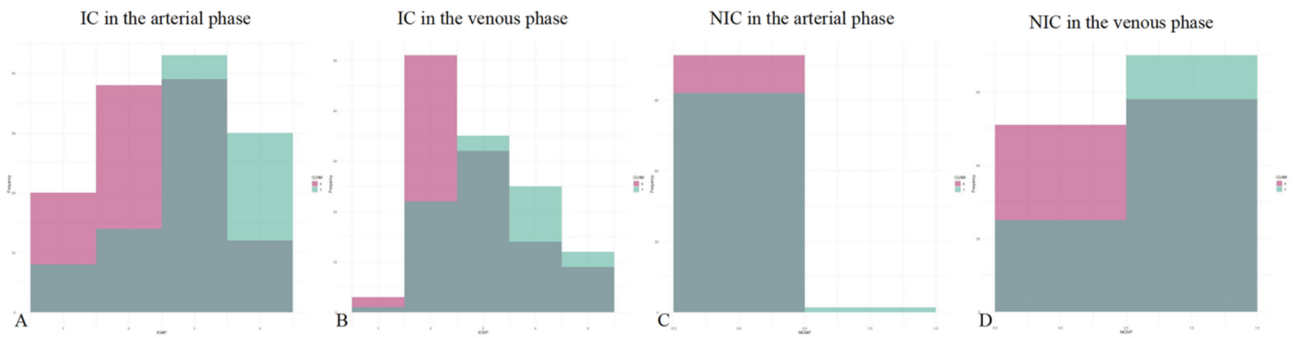


**Figure S2** Histogram of the distribution of continuous variables in the training cohort. IC, iodine concentration; NIC, normalized iodine concentration.

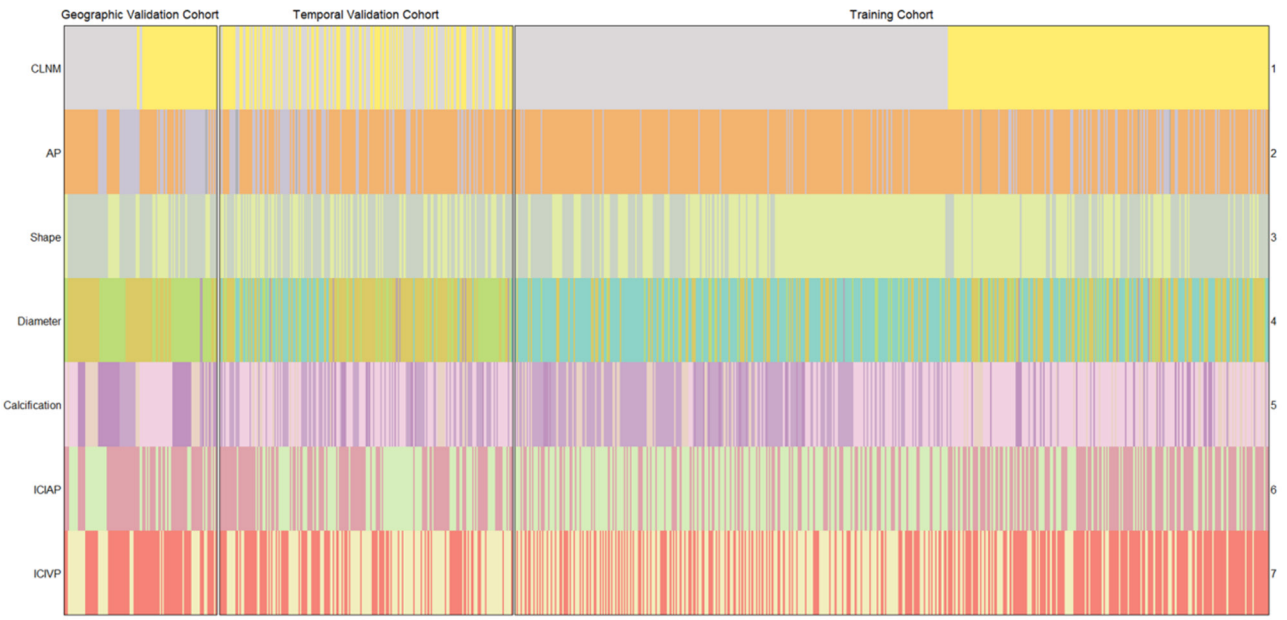


**Figure S3** Heat map of data distribution in the three cohorts.


https://dx.doi.org/10.21037/qims-24-284

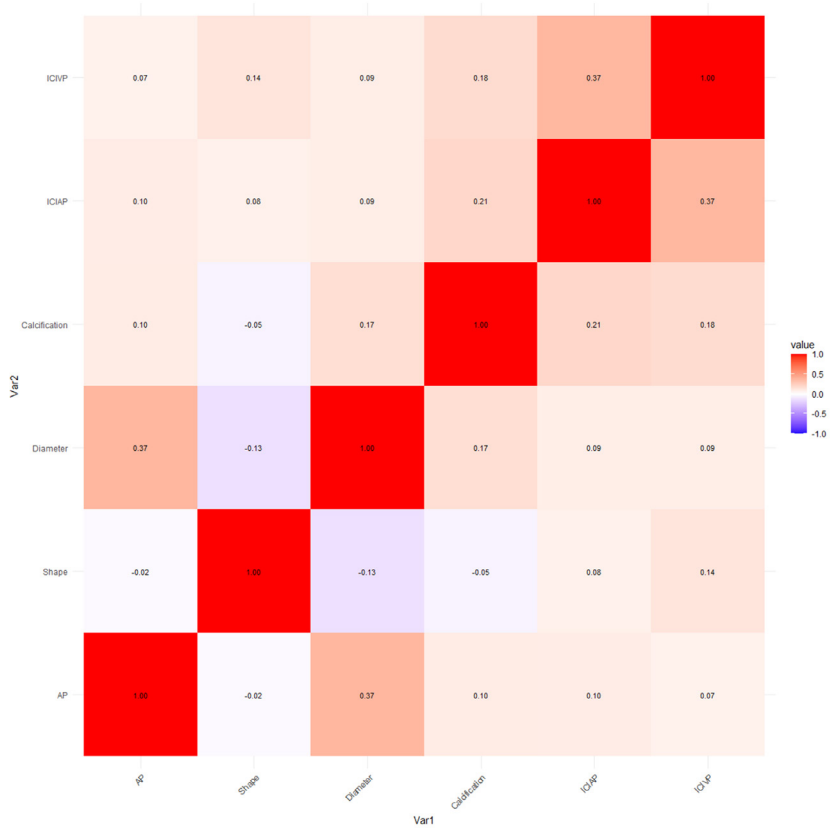


**Figure S4** Spearman correlation coefficient heat map of the variables included in the training cohort.


https://dx.doi.org/10.21037/qims-24-284

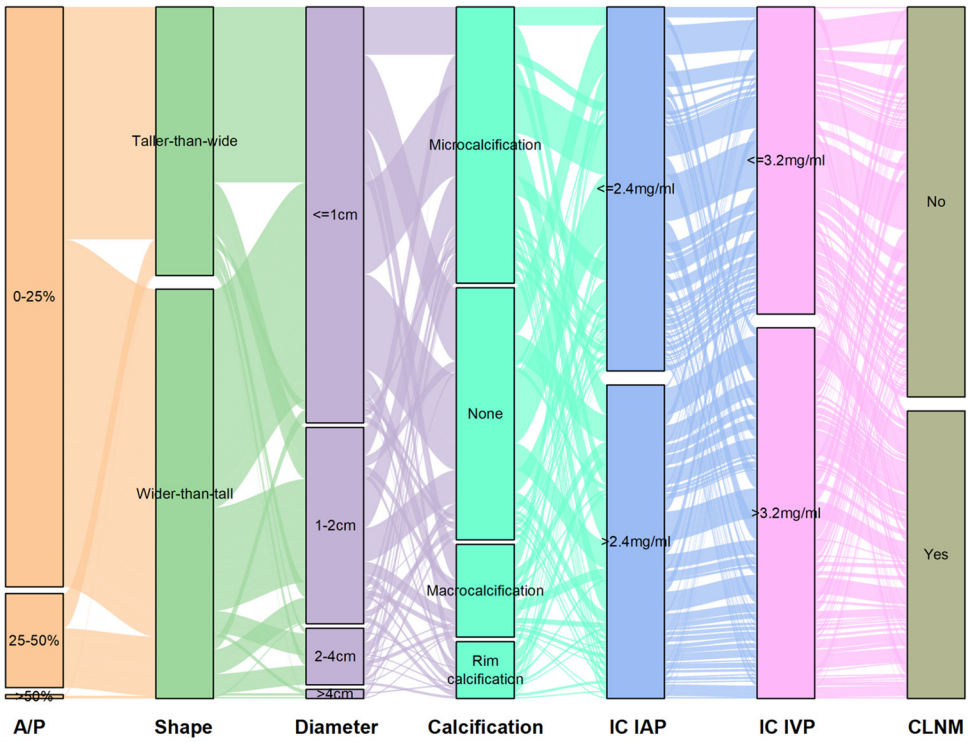


**Figure S5** The Sankey plot of the patients in the training cohort. All patients were divided into CLNM (–) and CLNM (+) through the six independent risk factors (A/P, shape, diameter, calcification, IC IAP, and IC IVP) in the training cohort. A/P, the ratio of capsular abutment over the lesion perimeter; CLNM, central lymph node metastasis; IAP, in the arterial phase; IC, iodine concentration; IVP, in the venous phase.


https://dx.doi.org/10.21037/qims-24-284

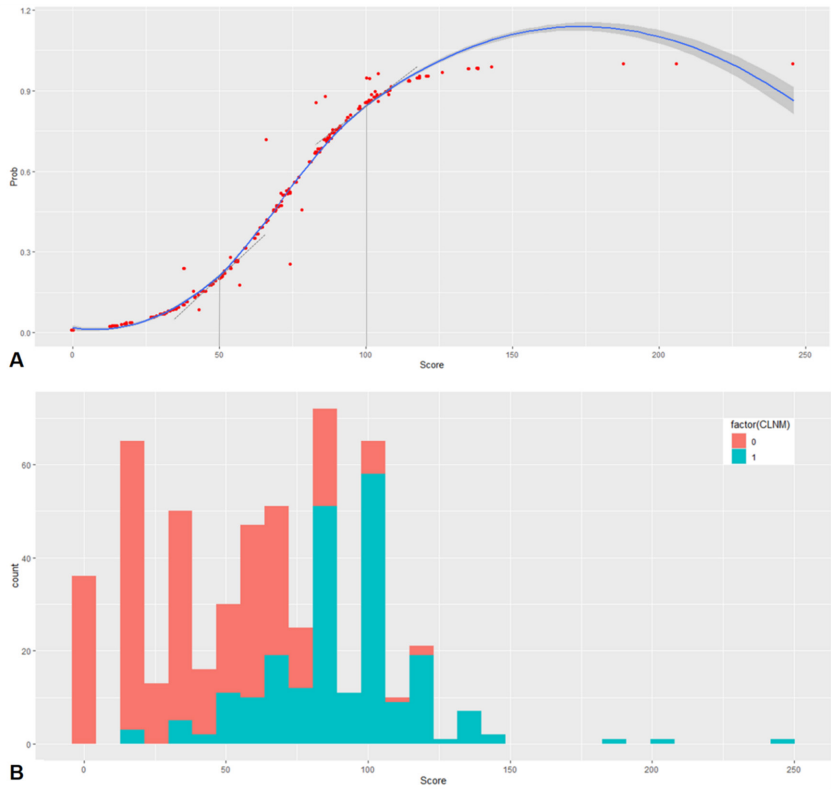


**Figure S6** The LOESS curve and histogram for risk stratification. (A) The LOESS curve was drawn to classify all patients into the low-, intermediate-, and high-risk groups for risk stratification based on the inflection points. (B) The distribution of patient scores in the histogram. LOESS, locally weighted regression.

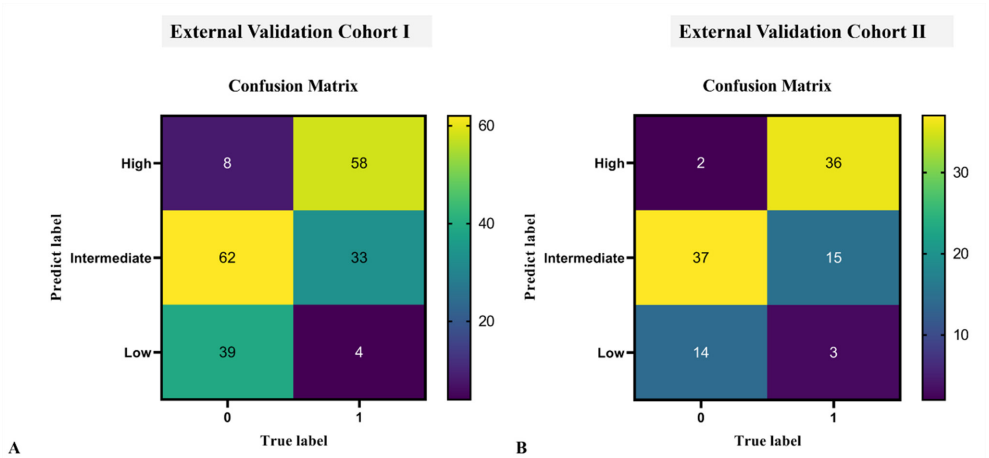


**Figure S7** The confusion matrix of the nomogram in the two external validation cohorts. In the external validation cohort I, the confusion matrix revealed that the possibility of CLNM was 9.3% (4/43), 34.7% (33/95), and 87.9% (58/66) in low-risk, intermediate-risk, and high-risk groups, respectively. In the external validation cohort II, the confusion matrix revealed that the possibility of CLNM was 17.6% (3/17), 28.8% (15/52), and 94.7% (36/38) in low-risk, intermediate-risk, and high-risk groups, respectively. CLNM, central cervical lymph node metastasis.


https://dx.doi.org/10.21037/qims-24-284

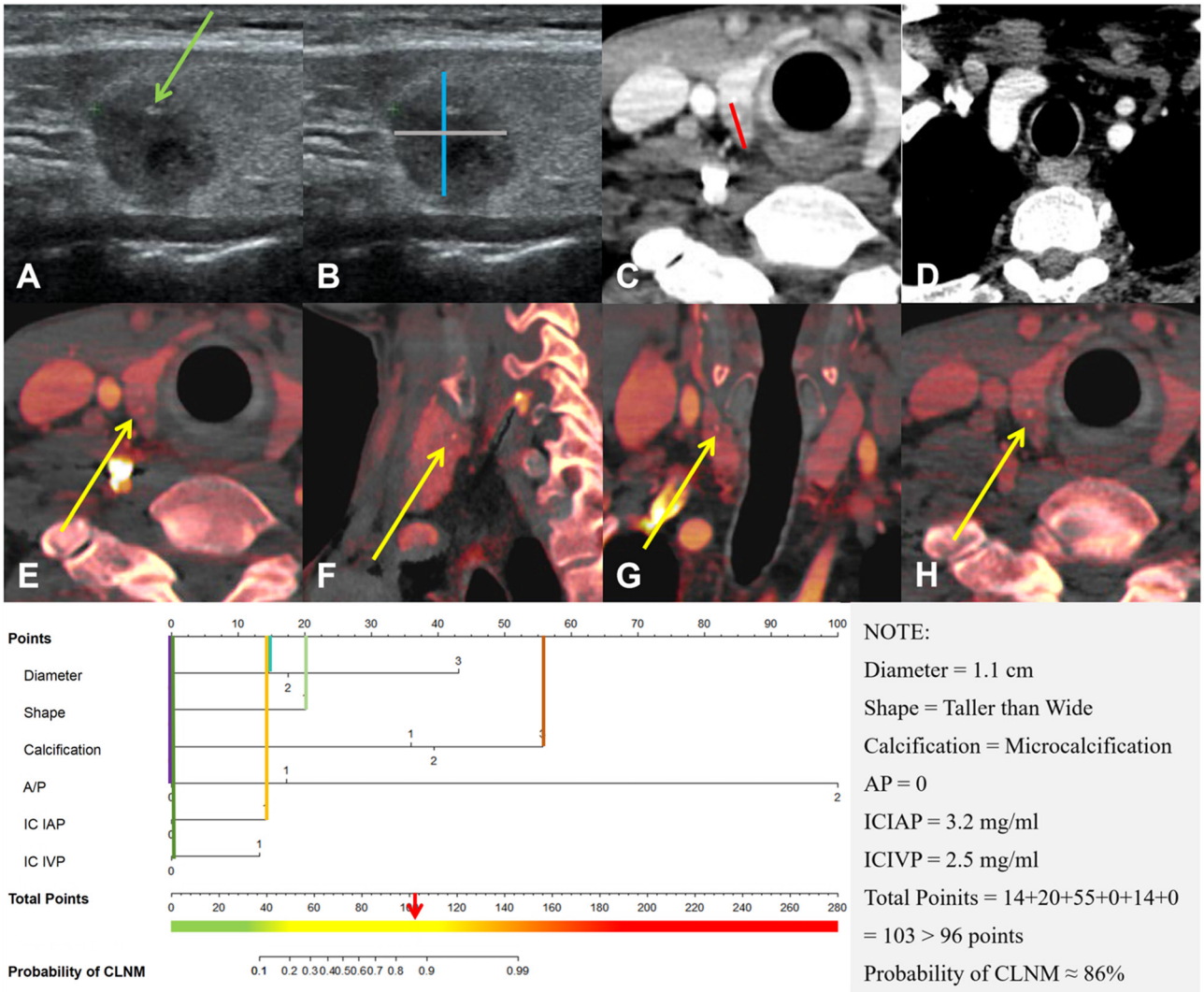


**Figure S8** An example of using the novel nomogram to illustrate the overestimation of individual risk of CLNM in patients with PTC. Female, 36 years old. Ultrasound manifestation: hypo-echo in the superior pole of the right lobe of the thyroid with a diameter of 1.1 cm, with microcalcification (A, green arrow), taller-than-wide (B), and A/P =0. On the iodine map of DECT, the IC in the arterial (E-G) and venous (H) phases of the measured lesion was 3.2 and 2.5 mg/mL, respectively. The total points =14+20+55+0+14+0=103 points >100 points, considered as a high-risk patient. However, postoperative pathological results showed that (right lobe) PTC, the diameter was 1.2 cm, no metastatic carcinoma was found in the central cervical region. This image is published with the patient's consent. (B) Taller-than-wide was defined as the anteroposterior diameter of the nodule (blue line) that was larger than its transverse diameter (gray line) on a transverse plane. The yellow arrows in (E-H) pointed to the thyroid primary lesions in the iodine maps of the arterial (E-G) and the venous (H) phases. Combining the axial (E), sagittal (F), and coronal (G) images, the primary lesion with the largest cross-sectional area was selected to measure. The region of interest was placed on the substantial part as large as possible, pay attention to avoid cystic degeneration, necrosis, or calcification, and not involve adjacent blood vessels. A/P, the ratio of capsular abutment over the lesion perimeter; CLNM, central lymph node metastasis; CT, computed tomography; IAP, in the arterial phase; IC, iodine concentration; IVP, in the venous phase; PTC, papillary thyroid carcinoma.


https://dx.doi.org/10.21037/qims-24-284

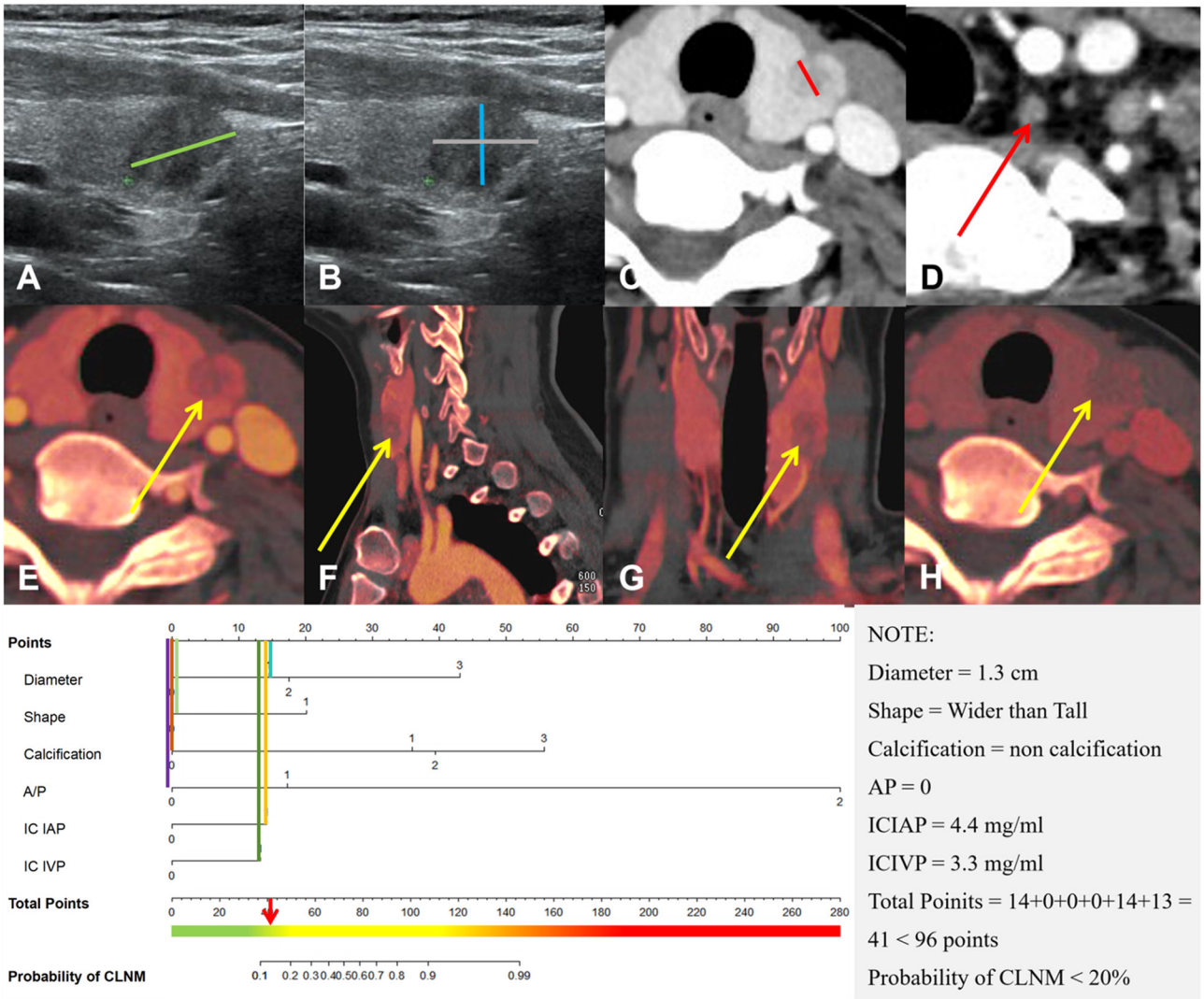


**Figure S9** An example of using the novel nomogram to illustrate the underestimation of individual risk of CLNM in patients with PTC. Male, 53 years old. Ultrasound manifestation: hypo-echo in the middle of the left lobe of the thyroid with a diameter of 1.3 cm (A, green line), with non-calcification, wider-than-tall (B), and A/P =0. On the iodine map of DECT, the IC in the arterial (E-G) and venous (H) phases of the measured lesion was 4.4 and 3.3 mg/mL, respectively. The total points =14+0+0+0+14+13=41 points <50 points, considered as a low-risk patient. However, postoperative pathological results showed that (left lobe) PTC, the diameter was 1.3 cm, metastatic carcinoma were found (2/2) in the central cervical region. This image is published with the patient's consent. (B) Wider-than-tall was defined as the anteroposterior diameter of the nodule (blue line) that was smaller than its transverse diameter (gray line) on a transverse plane. The yellow arrows in (E-H) pointed to the thyroid primary lesions in the iodine maps of the arterial (E-G) and the venous (H) phases. Combining the axial (E), sagittal (F), and coronal (G) images, the primary lesion with the largest cross-sectional area was selected to measure. The region of interest was placed on the substantial part as large as possible, pay attention to avoid cystic degeneration, necrosis, or calcification, and not involve adjacent blood vessels. A/P, the ratio of capsular abutment over the lesion perimeter; CLNM, central lymph node metastasis; CT, computed tomography; IAP, in the arterial phase; IC, iodine concentration; IVP, in the venous phase; PTC, papillary thyroid carcinoma.


https://dx.doi.org/10.21037/qims-24-284

**Table S1** The other baseline information of ultrasound and DECT in the training cohort

| Variables | Training cohort | | | |
|---|---|---|---|---|
| | Total (n=525) | CLNM (–) (n=302) | CLNM (+) (n=223) | P |
| Demographics | | | | |
| Sex | | | | 0.055[§] |
| Male | 122 (23.2) | 61 (20.2) | 61 (27.4) | |
| Female | 403 (76.8) | 241 (79.8) | 162 (72.6) | |
| Age[†] | | | | 0.555[¶] |
| ≤55 years | 415 (79.0) | 236 (78.1) | 179 (80.3) | |
| >55 years | 110 (21.0) | 66 (21.9) | 44 (19.7) | |
| Ultrasound | | | | |
| Location | | | | 0.122[§] |
| Left lobe | 216 (41.1) | 129 (42.7) | 87 (39.0) | |
| Right lobe | 261 (49.7) | 152 (50.3) | 109 (48.9) | |
| Isthmus | 48 (9.1) | 21 (7.0) | 27 (12.1) | |
| Composition[‡] | | | | 0.623[§] |
| Cystic | 2 (0.4) | 1 (0.3) | 1 (0.4) | |
| Spongiform | 6 (1.1) | 5 (1.7) | 1 (0.4) | |
| Mixed | 20 (3.8) | 12 (4.0) | 8 (3.6) | |
| Solid | 497 (94.7) | 284 (94.0) | 213 (95.5) | |
| Margin[‡] | | | | 0.022[§] |
| Smooth | 31 (5.9) | 23 (7.6) | 8 (3.6) | |
| Ill-defined | 52 (9.9) | 36 (11.9) | 16 (7.2) | |
| Lobulated or irregular | 442 (84.2) | 243 (80.5) | 199 (89.2) | |
| Echogenictiy[‡] | | | | 0.320[§] |
| Anechoic | 4 (0.8) | 2 (0.7) | 2 (0.9) | |
| Hyper/isoechoic | 6 (1.1) | 4 (1.3) | 2 (0.9) | |
| Hypoechoic | 474 (90.3) | 267 (88.4) | 207 (92.8) | |
| Very hypoechoic | 41 (7.8) | 29 (9.6) | 12 (5.4) | |
| DECT | | | | |
| NIC IAP | 0.25±0.09 | 0.23±0.09 | 0.29±0.08 | < 0.001[⊥] |
| NIC IVP | 0.57±0.17 | 0.54±0.17 | 0.62±0.17 | < 0.001[⊥] |

[†], according to the 8th AJCC staging systems. [‡], refer to American College of Radiology Thyroid Imaging, Reporting, and Data for grouping criteria. [§], categorical variables were represented by number (frequency) using Mann-Whitney U test. [¶], continuous variables that did not fit to the normal distribution were represented by number (frequency), using the Kolmogorov-Smirnov test. [⊥], continuous variables that fitted to the normal distribution were represented by mean ± standard deviation, using the Kolmogorov-Smirnov test. AJCC, American Joint Committee on Cancer; CLNM, central lymph node metastasis; DECT, dual-energy computed tomography; IAP, in the arterial phase; IVP, in the venous phase; NIC, normalized iodine concentration.


https://dx.doi.org/10.21037/qims-24-284

**Table S2** Baseline information of ultrasound and DECT in the external validation cohort I

| Variables, N (%) | External validation cohort I | | | |
|---|---|---|---|---|
| | Total (n=204) | CLNM (–) (n=109) | CLNM (+) (n=95) | P |
| Demographics | | | | |
| Sex | | | | 0.005[¶] |
| Male | 58 (28.4) | 32 (20.2) | 36 (37.9) | |
| Female | 146 (71.6) | 87 (79.8) | 59 (62.1) | |
| Age[†] | | | | 0.279[⊥] |
| ≤55 years | 163 (79.9) | 84 (77.1) | 79 (83.2) | |
| >55 years | 41 (20.1) | 25 (22.9) | 16 (16.8) | |
| Ultrasound | | | | |
| Diameter[†] | | | | <0.001[⊥] |
| T1a | 47 (23.0) | 38 (34.9) | 9 (9.5) | |
| T1b | 102 (50.0) | 57 (52.3) | 45 (47.4) | |
| T2 | 48 (23.5) | 13 (11.9) | 35 (36.8) | |
| ≥ T3 | 7 (3.4) | 1 (0.9) | 6 (6.3) | |
| Shape[‡] | | | | <0.001[¶] |
| Wider-than-tall | 108 (52.9) | 85 (78.0) | 23 (24.2) | |
| Taller-than-wide | 96 (47.1) | 24 (22.0) | 72 (75.8) | |
| Calcification[‡] | | | | <0.001[¶] |
| None or large comet-tail | 80 (39.2) | 62 (56.9) | 18 (18.9) | |
| Macrocalcification | 16 (7.8) | 15 (13.8) | 1 (1.1) | |
| Rim calcification | 11 (5.4) | 11 (10.1) | 0 | |
| Microcalcification | 97 (47.5) | 21 (19.3) | 76 (90.0) | |
| A/P[§] | | | | <0.001[⊥] |
| <25% | 159 (77.9) | 97 (89.0) | 62 (65.3) | |
| 25–50% | 42 (20.6) | 10 (9.2) | 32 (33.7) | |
| >50% | 3 (1.5) | 2 (1.8) | 1 (1.1) | |
| DECT | | | | |
| IC IAP (mg/mL) | 2.72±0.91 | 2.44±0.86 | 3.05±0.86 | <0.001[#] |
| IC IVP (mg/mL) | 3.07±0.99 | 2.85±0.97 | 3.33±0.97 | <0.001[#] |
| NIC IAP | 0.25±0.09 | 0.23±0.29 | 0.29±0.88 | <0.001[#] |
| NIC IVP | 0.59±0.19 | 0.55±0.18 | 0.64±0.19 | <0.001[#] |

[†], according to the 8th AJCC staging systems. [‡], refer to American College of Radiology Thyroid Imaging, Reporting, and Data for grouping criteria. [§], A/P was graded by values of <25%, 25–50%, or >50%, proven by a previous study. [¶], categorical variables were represented by number (frequency) using Mann-Whitney U test. [⊥], continuous variables that did not fit to the normal distribution were represented by number (frequency), using the Kolmogorov-Smirnov test. [#], continuous variables that fitted to the normal distribution were represented by mean ± standard deviation, using the Kolmogorov-Smirnov test. AJCC, American Joint Committee on Cancer; A/P, the ratio of capsular abutment over the lesion perimeter; CLNM, central lymph node metastasis; DECT, dual-energy computed tomography; IAP, in the arterial phase; IC, iodine concentration; IVP, in the venous phase; NIC, normalized iodine concentration.


https://dx.doi.org/10.21037/qims-24-284

**Table S3** Baseline information of ultrasound and DECT in the external validation cohort II

| Variables, N (%) | External validation cohort II | | | |
|---|---|---|---|---|
| | Total (n=107) | CLNM (–) (n=53) | CLNM (+) (n=54) | P |
| Demographics | | | | |
| Sex | | | | 0.091[¶] |
| Male | 38 (35.5) | 23 (43.4) | 15 (27.8) | |
| Female | 69 (64.5) | 30 (56.6) | 39 (72.2) | |
| Age[†] | | | | 0.759[⊥] |
| ≤55 years | 90 (84.1) | 44 (83.0) | 46 (85.2) | |
| >55 years | 17 (15.9) | 9 (17.0) | 8 (14.8) | |
| Ultrasound | | | | |
| Diameter[†] | | | | 0.030[⊥] |
| T1a | 52 (48.6) | 32 (60.4) | 20 (37.0) | |
| T1b | 53 (49.5) | 21 (39.6) | 32 (59.3) | |
| T2 | 2 (1.9) | 0 | 2 (3.7) | |
| ≥ T3 | 0 | 0 | 0 | |
| Shape[‡] | | | | 0.153[¶] |
| Wider-than-tall | 31 (29.0) | 12 (22.6) | 19 (35.2) | |
| Taller-than-wide | 76 (71.0) | 41 (77.4) | 35 (64.8) | |
| Calcification[‡] | | | | 0.170[¶] |
| None or large comet-tail | 17 (15.9) | 11 (20.8) | 6 (11.1) | |
| Macrocalcification | 22 (20.6) | 11 (20.8) | 11 (20.4) | |
| Rim calcification | 36 (33.6) | 20 (37.7) | 16 (29.6) | |
| Microcalcification | 32 (29.9) | 11 (20.8) | 21 (38.9) | |
| A/P[§] | | | | 0.089[⊥] |
| <25% | 60 (56.1) | 35 (66.0) | 25 (46.3) | |
| 25–50% | 46 (43.0) | 18 (34.0) | 28 (51.9) | |
| >50% | 1 (0.9) | 0 | 1 (1.9) | |
| DECT | | | | |
| IC IAP (mg/mL) | 2.64±0.63 | 2.55±0.57 | 2.74±0.67 | <0.001[#] |
| IC IVP (mg/mL) | 3.41±0.62 | 3.22±0.62 | 3.60±0.56 | <0.001[#] |
| NIC IAP | 0.22±0.06 | 0.17±0.27 | 0.27±0.31 | <0.001[#] |
| NIC IVP | 0.57±0.06 | 0.51±0.23 | 0.62±0.35 | <0.001[#] |

[†], according to the 8th AJCC staging systems. [‡], refer to American College of Radiology Thyroid Imaging, Reporting, and Data for grouping criteria. [§], A/P was graded by values of <25%, 25–50%, or >50%, proven by a previous study. [¶], categorical variables were represented by number (frequency) using Mann-Whitney U test. [⊥], continuous variables that did not fit to the normal distribution were represented by number (frequency), using the Kolmogorov-Smirnov test. [#], continuous variables that fitted to the normal distribution were represented by mean ± standard deviation, using the Kolmogorov-Smirnov test. AJCC, American Joint Committee on Cancer; A/P, the ratio of capsular abutment over the lesion perimeter; CLNM, central lymph node metastasis; DECT, dual-energy computed tomography; IAP, in the arterial phase; IC, iodine concentration; IVP, in the venous phase; NIC, normalized iodine concentration.


https://dx.doi.org/10.21037/qims-24-284

**Table S4** The result of consistency analysis in the three cohorts

| Parameters | Training cohort | | External validation cohort I | | External validation cohort II | |
|---|---|---|---|---|---|---|
| | ICC (95% CI) | P | ICC (95% CI) | P | ICC (95% CI) | P |
| Diameter | | | | | | |
| Radiologist A | 0.999 (0.998–0.999) | <0.001 | 0.997 (0.997–0.998) | <0.001 | 0.943 (0.921–0.956) | <0.001 |
| Radiologist B | 0.998 (0.997–0.998) | <0.001 | 0.995 (0.994–0.996) | <0.001 | 0.937 (0.911–0.949) | <0.001 |
| Radiologists A and B | 0.988 (0.984–0.995) | <0.001 | 0.930 (0.916–0.942) | <0.001 | 0.912 (0.896–0.932) | <0.001 |
| IC IAP | | | | | | |
| Radiologist C | 0.980 (0.974–0.985) | <0.001 | 0.975 (0.969–0.979) | <0.001 | 0.933 (0.917–0.951) | <0.001 |
| Radiologist D | 0.968 (0.958–0.975) | <0.001 | 0.961 (0.952–0.967) | <0.001 | 0.949 (0.928–0.953) | <0.001 |
| Radiologists C and D | 0.972 (0.963–0.978) | <0.001 | 0.971 (0.965–0.976) | <0.001 | 0.924 (0.909–0.937) | <0.001 |
| IC IVP | | | | | | |
| Radiologist C | 0.941 (0.924–0.955) | <0.001 | 0.944 (0.932–0.953) | <0.001 | 0.929 (0.913–0.942) | <0.001 |
| Radiologist D | 0.936 (0.918–0.951) | <0.001 | 0.937 (0.924–0.948) | <0.001 | 0.918 (0.901–0.931) | <0.001 |
| Radiologists C and D | 0.965 (0.955–0.973) | <0.001 | 0.960 (0.975–0.983) | <0.001 | 0.903 (0.883–0.923) | <0.001 |

A and B were two radiologists with over 10 years of work experience in ultrasound diagnosis; C and D were another two radiologists with more than 10 decades of work experience in CT diagnosis. CI, confidence interval; IAP, in the arterial phase; IC, iodine concentration; ICC, intraclass correlation coefficient; IVP, in the venous phase.

**Table S5** Predictive efficacy of quantitative parameters on CLNM in patients with PTC

| Parameters | Cutoff value | AUC (95% CI) | P |
|---|---|---|---|
| IC IAP (mg/mL) | >2.4 | 0.714 (0.673–0.752) | <0.001 |
| IC IVP (mg/mL) | >3.2 | 0.703 (0.662–0.742) | <0.001 |
| NIC IAP | >0.21 | 0.680 (0.638–0.720) | <0.001 |
| NIC IVP | >0.55 | 0.649 (0.606–0.689) | <0.001 |

AUC, area under the curve; CI, confidence interval; CLNM, central lymph node metastasis; IAP, in the arterial phase; IC, iodine concentration; IVP, in the venous phase; NIC, normalized iodine concentration; PTC, papillary thyroid carcinoma.

**Table S6** Multicollinearity assessment in the nomogram based on the independent predictors

| Predictors | Collinearity statistics | |
|---|---|---|
| | Tolerance | VIF |
| Diameter | 0.795 | 1.258 |
| Shape | 0.953 | 1.049 |
| Calcification | 0.922 | 1.084 |
| A/P | 0.819 | 1.220 |
| IC IAP | 0.837 | 1.195 |
| IC IVP | 0.834 | 1.199 |

A/P, the ratio of capsular abutment over the lesion perimeter; IAP, in the arterial phase; IC, iodine concentration; IVP, in the venous phase; VIF, variance inflation factor.


https://dx.doi.org/10.21037/qims-24-284

**Table S7** The calibration efficiency of the nomogram in the three cohorts

| | MAE | MSE | 0.9 QoAB |
|---|---|---|---|
| Training Cohort (n=525) | 0.015 | 0.00036 | 0.029 |
| External Validation Cohort I (n=204) | 0.033 | 0.00169 | 0.062 |
| External Validation Cohort II (n=107) | 0.051 | 0.00378 | 0.101 |

MAE, mean absolute error; MSE, mean squared error; QoAB, quantile of absolute error.

**Table S8** Evaluation of the risk prediction model concerning NRI and IDII in the three cohorts

| | Model 1 *vs.* Model 2[†] | P |
|---|---|---|
| Training cohort | | |
| Categorical NRI (95% CI) | 0.1277 (0.0519–0.2035) | 0.00096 |
| Continuous NRI (95% CI) | 0.6851 (0.4529–0.9172) | <0.001 |
| IDII (95% CI) | 0.0702 (0.0352–0.1052) | <0.001 |
| External validation cohort I | | |
| Categorical NRI (95% CI) | 0.1908 (0.1034–0.2782) | <0.001 |
| Continuous NRI (95% CI) | 0.587 (0.3239–0.85) | <0.001 |
| IDII (95% CI) | 0.0962 (0.0611–0.1314) | <0.001 |
| External validation cohort II | | |
| Categorical NRI (95% CI) | 0.1663 (0.0564–0.2762) | 0.00301 |
| Continuous NRI (95% CI) | 0.827 (0.5013–1.1528) | <0.001 |
| IDII (95% CI) | 0.1706 (0.1093–0.2319) | <0.001 |

[†], Model 1: the prediction model based on combined ultrasound and DECT parameters; Model 2: the prediction model based on ultrasound parameters only. CI, confidence interval; DECT, dual-energy computed tomography; IDII, integrated discrimination improvement index; NRI, net reclassification improvement.


https://dx.doi.org/10.21037/qims-24-284